Nuclear Instruments and Methods in Physics Research A286 (1990) 135–146
North-Holland

A STUDY OF THE ELECTRON IMAGE DUE TO IONIZING EVENTS IN A TWO-DIMENSIONAL LIQUID ARGON TPC WITH A 24 cm DRIFT GAP

S. BONETTI [3], A. BRAGGIOTTI [4], E. BUCKLEY [2]+, M. CAMPANELLA [3], G. CARUGNO [1], G. CECCHET [5], P. CENNINI [1], S. CENTRO [4], A. CIOCIO [2], S. CITTOLIN [1], B. DAINESE [4], M. FERRO-LUZZI [1], F. GASPARINI [4]**, A. GONIDEC [1], P.F. MANFREDI [3], E. MERONI [3], R. MUÑOZ [1], J-M. PERREAU [1], F. PIETROPAOLO [4], F. PTOHOS [1]*, F. RAGUSA [3], P. ROSSI [4], C. RUBBIA [1], D. SCHINZEL [1], W.F. SCHMIDT [1]++ and W. SEIDL [1]

[1] *CERN, CH-1211, Geneva 23, Switzerland*
[2] *Laboratori Nazionali di Frascati, Via Enrico Fermi 40, Frascati, Rome, Italy*
[3] *Dipartimento di Fisica and Sezione dell'INFN, Università di Milano, Via Celoria 16, Milano, Italy*
[4] *Dipartimento di Fisica and Sezione dell'INFN, Univ. di Padova, Via F. Marzolo 8, Padova, Italy*
[5] *Dipartimento di Fisica and Sezione dell'INFN, Univ. di Pavia, Via A. Bassi 6, Pavia Italy*

Received 4 September 1989

We have tested a liquid argon time projection chamber with a novel wire configuration based on electrostatic focussing which allows the realization of a nondestructive detection of the electron image produced by ionizing events. The chamber was tested in a 5 GeV pion beam at the CERN proton synchrotron. The measured pulse shapes at both 200 V/cm and 500 V/cm were in very good agreement with the expected shapes, calculated taking into account the electron lifetime, the response of the electronics and the longitudinal diffusion of the electron cloud. The measured electron drift velocity was in good agreement with the results of other workers as well as with our previous measurements.

We have also analysed a sample of events containing delta rays in order to study the behaviour of low-energy electrons in the liquid argon. We find that for electron energies greater than 5 MeV the measured energy spectrum agrees very well with the predicted spectrum after corrections for acceptance and energy loss, hence demonstrating the feasibility of recognizing low-energy electrons in liquid argon.

1. Introduction

Since the initial proposal for a liquid argon time projection chamber in 1977 [1], much work has been done by different groups towards realizing this kind of device [2–7]. Liquid argon is ideal for the detection of rare events because of its high density and its ability to be both target and detector. In particular, the proposed ICARUS detector [8] is a large-volume liquid argon TPC which will be situated in the Gran Sasso Underground Laboratory in Italy and will study primarily solar neutrino interactions.

In a detector such as this it is desirable to reduce the number of detection planes to a minimum. This implies very long drift lengths, of the order of 2 m, meaning that the liquid argon has to be free electronegative impurities at a level of < 1 ppb. We have previously demonstrated that it is possible to obtain ultrapure liquid argon with an electron lifetime in the region of 9 ms (0.03 ppb oxygen equivalent) [9], using a simple purification system consisting of a mixture of molecular sieve and silica gel together with an Oxisorb cartridge [10] to remove oxygen. The design for the purification system was chosen as a result of the experience gained in cleaning warm liquids at CERN in connection with the new UA1 calorimeter [11].

As part of the continuing development program for the ICARUS experiment, we have successfully tested a two-dimensional liquid argon TPC with a 24 cm drift gap. The chamber consisted of a single detection plane in the form of a grid of sense-wires. The wires plus the drift time provided a two-dimensional electron image of tracks produced in the drift volume. With this chamber

+ Present address: Physics Department, Rutgers University, Piscataway, NJ 08855-0849, USA.
++ Visiting scientist 1986/1987 from the Hahn-Meitner Institut, Berlin, FRG.
* Present address: High Energy Physics Laboratory, Harvard University, Cambridge, MA 02138, USA.
** Present address: Dipartimento di Fisica and Sezione dell' INFN, Università di Udine, Via Larga 36, Udine, Italy.

0168-9002/90/$03.50

we have demonstrated that the theory of charge induction on a grid of wires in a liquid noble gas works in practice, hence the idea of a nondestructive readout has been realized for the first time. We note here that the group of Chen have also reported results from a two-dimensional TPC, but their readout plane consisted of strips 2.5 mm apart etched on copper-plated G-30, rather than a grid of wires [4].

The chamber was tested in a 5 GeV pion beam at the CERN proton synchrotron. This provided a much higher event rate than cosmic rays and allowed us to determine accurately the energy and direction of the incoming particle. To test the feasibility of identifying low-energy electrons, we have studied the production of delta rays in the chamber and measured their energy spectrum.

The paper is organized in the following way. In section 2 we explain the improvements we have made to the original design for a liquid argon TPC [1,6]. We then describe the chamber constructed using this idea. In section 3 we give a brief summary of the purification system, as this has been explained in detail in a previous publication [9]. Section 4 deals with the electronics, the data acquisition and the experimental setup. In section 5 we discuss the chamber performance and results, and in section 6 we present our conclusions.

2. The chamber design

The theory of electron imaging of ionizing events occurring inside the sensitive volume of a liquid argon TPC and the design of such a chamber was developed by Gatti and co-workers [6]. The basic design consisted of a screen-grid of equally spaced parallel wires, and a sense-wire grid also of equally spaced parallel wires of the same pitch, placed at a distance W from the screen-grid. This arrangement produces a two-dimensional electron image, one coordinate is provided by the position of the hit wires and the other by the drift time. For a three-dimensional image, a second sense-wire grid is placed at 90° to the first. The presence of the screen-grid means that a signal is not induced on the sense-wires until the drifting electrons cross the grid. The grid will be 100% transparent to the drifting electrons if the following conditions is satisfied [12]:

$$E_A/E_B > (1+x)/(1-x), \quad (1)$$

where E_A is the field after the grid, E_B is the field before the grid and

$$x = 2\pi r/d, \quad (2)$$

where r is the wire radius and d is the distance between the wire centres. The principles of operation of this system have been extensively described in ref. [6] and will not be discussed further.

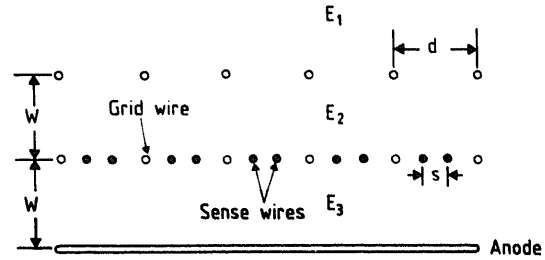

Fig. 1. The wire configuration used in the chamber described in the text. The dimensions are: $W = 2$ mm, $d = 2$ mm, $s = 0.5$ mm, R(grid-wire) = 50 μm, and R (sense-wire) = 25 μm).

The original design suffered from two main problems. The first was that non-negligible signals were induced on one sense-wire from electrons drifting towards the neighbouring sense-wire. One had to move at least three sense-wire gaps away before this signal became negligible. The second problem was nonuniformity in shape and magnitude of the induced signals, which depended strongly on the position of the drifting electrons with respect to the sense-wires.

In designing the chamber, we have modified the original design to obtain a wire arrangement that significantly reduces both of the above problems. This is shown schematically in fig. 1. We have replaced the single sense-wire plane with a plane containing pairs of sense-wires separated by a distance s, with an extra wire in between each pair which acts as a shield between the sense-wires. We retain the screen-grid as before. The electric fields in the drift space, screen-grid/sense-wire gap and sense-wire/anode gap are represented by E_1, E_2, E_3 respectively. For electric field E_2 larger than E_1 the field lines are focussed towards the sense-wires. If the electric field E_3 is chosen to be the correct value, then the field lines pass between the sense-wires and end on the anode. For a three-dimensional chamber, the field lines can pass to a second sense-wire plane hence realizing a nondestructive readout.

We have investigated different choices of the wire diameters and spacings and our final choice is $W = 2$ mm, $d = 2$ mm, $s = 0.5$ mm, $R_{GW} = 50$ μm, $R_{SW} = 25$ μm, where R_{GW} and R_{SW} are the radii of the grid-wires and the sense-wires respectively. For these parameters, the transparency of the screen-grid is 100% if the ratio of the fields after and before the grid, E_2/E_1, is at least 1.4. However, in order to focus the field lines so that the sense-wires are 100% transparent, it is required that $E_2/E_1 \geq 3$. We have considered two possible configurations for the electric fields that satisfy this criteria, namely $E_1 : E_2 : E_3 \equiv 1 : 3 : 9$ and $E_1 : E_2 : E_3 \equiv 1 : 5 : 5$. We have developed a drift chamber simulation program that allows us to calculate the potential map, the electron trajectories and the signal shapes for a particular wire-configuration. The calculations made with this pro-

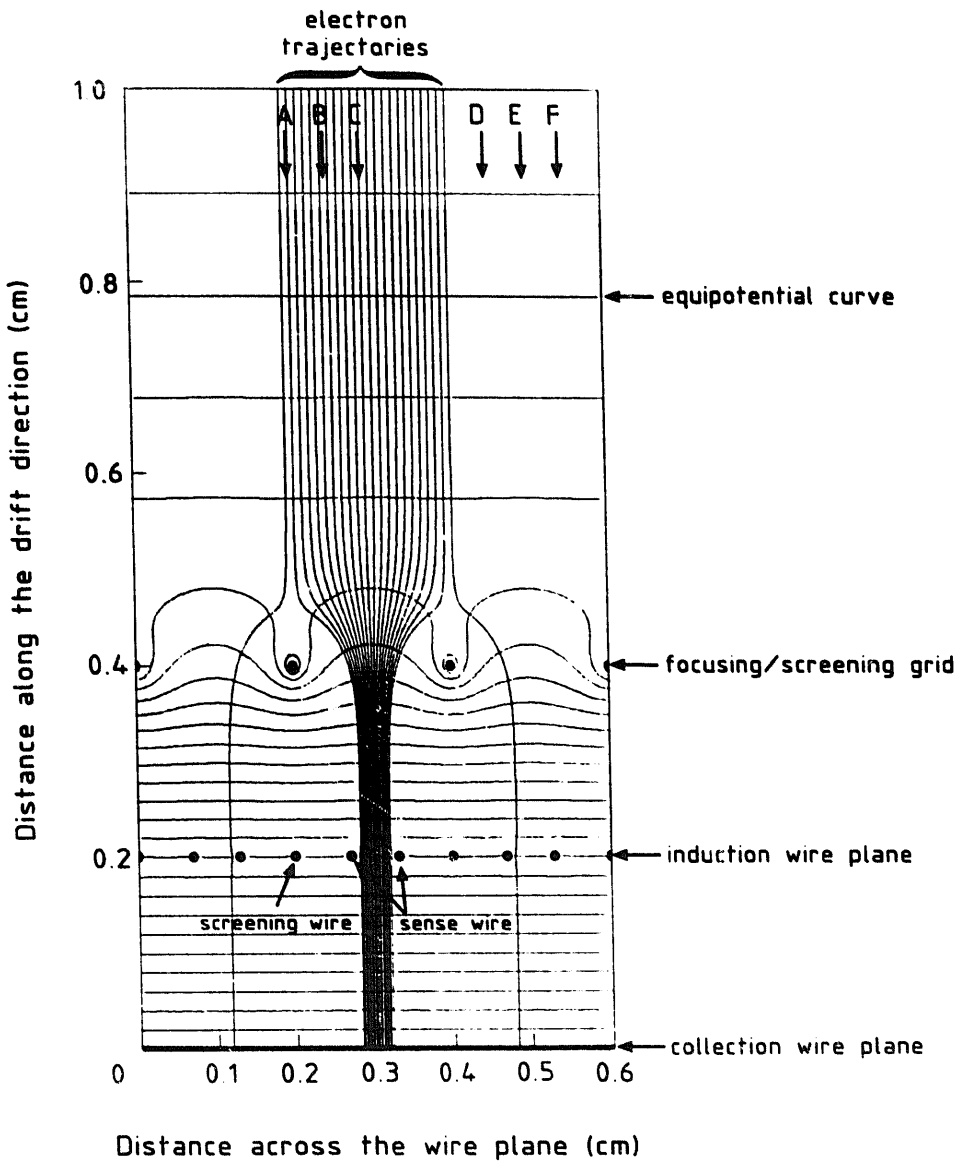

Fig. 2. The electric field map including the equipotential lines for the wire configuration in fig. 1 and the ratio of fields of $E_1 : E_2 : E_3 \equiv 1 : 5 : 5$.

gram suggest that the second field-configuration has better focussing properties and a simpler potential distribution with the screen-grid sitting at the natural potential given by the field while the sense-wires and shielding wires are at ground. The corresponding field map is shown in fig. 2 for the parameters given above. The shielding-inefficiency of the screen-grid, which is a function of the geometry only and not the electric field, is $\approx 10\%$ [12]. This inefficiency causes the sense-wires to see the drifting electrons before they cross the screen-grid, and results in a small tail at the beginning of the pulse.

As before, the signal induced on a single sense-wire varies according to the lateral position of the drifting electrons. However, for each pair of wires the sum of the two signals is almost constant as shown in fig. 3a, where the sum is plotted as a function of the position of the drifting electrons with respect to the grid-wires. We note that the induced signal never reaches 100%, the maximum value is $\approx 88\%$ and the mean value is $\approx 75\%$. This situation could be improved by using larger diameter wires or increased spacing between the screen-grid and the sense-wire grid. In fig. 3b we show the summed signals as a function of drift time for three positions of the drifting electrons, labelled A, B and C (as indicated in fig. 3a). The origin ($t = 0$) corresponds to the time when the electrons are in the drift volume at ≈ 3 mm from the screen-grid, while the maximum of the signals corresponds to the passage of the electrons through the induction plane. Even though the pairs of sense-wires

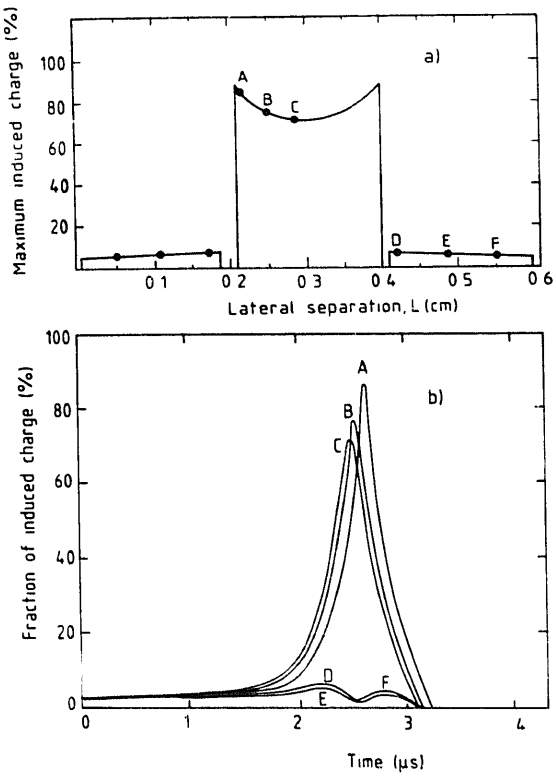

Fig. 3. Calculated signals induced in a pair of sense-wires in the induction plane by electrons drifting at various lateral position. (a) Maximum fraction of induced charge as a function of the lateral position of the drifting electrons. The points A, B, C, D, E, F correspond to six different electron trajectories, as defined in fig. 2. (b) Time dependence of the charge signal for the same six electron trajectories (A, B, C, D, E, F). This calculation has been made for $E_1 = 500$ V/cm and $v_d = 1.55$ mm μs^{-1}.

are shielded from each other by the grid-wires, the shielding is not 100%. This is illustrated by the curves labelled D, E and F in fig. 3b, which are the signals induced on the sense-wire (at positions D, E and F shown in fig. 3a) due to electrons drifting in the neighbouring cell. This contribution is $\leq 6\%$ and that from the next but one cell is essentially zero, an improvement over the original design.

A cross-section through the chamber is shown in fig. 4. All of the metal parts were constructed from stainless steel and were subjected to the CERN "standard cleaning procedure" which has been described in previous publications [9,13]. The chamber was constructed from a stainless steel cathode plate of 100×100 mm^2 which was joined to the wire plane by a series of 24 field-shaping rings, also 100×100 mm^2, of 3 mm thickness separated by 7 mm spacers of insulating material (PTFE). Each ring was connected to the next by a 60 MΩ ceramic resistor. The resistors had their coat of varnish removed and their leads were gold-plated to prevent corrosion during cleaining. The resistors were cleaned with soap and water plus ultrasound. The final resistor was connected from the screen-grid to ground, and it was possible to achieve the field ratio of 1 : 5 before and after the grid by using another 60 MΩ resistor. This racetrack ensured that the electric field inside the chamber was uniform. The grid- and sense-wires were stainless steel of 100 μm and 50 μm diameter respectively and were mounted in a MACOR [14] frame. There were 31 pairs of sense-wires. The distance between the screen-grid/sense-wire plane and the sense-wire plane/anode was 2 mm.

The high voltage was supplied through the bottom of the chamber via a ceramic feedthrough as can be seen in fig. 4. The chamber was contained in a stainless steel vessel, 388 mm long with DN160 ConFlat [15] flanges on the top and bottom, and the total volume of the chamber was 8.6 l. The top flange contained a single pipe for evacuation and filling of the chamber and four multi-pin cryogenic feedthroughs for the sense-wire readout. Each feedthrough read out eight pairs of sense-wires. There were three additional feedthroughs, one for the anode high voltage and signal, one for the screen-grid high voltage and one for the sense-grid voltage. These feedthroughs could also be used to supply a test pulse to the anode and the grids. In the field-con-

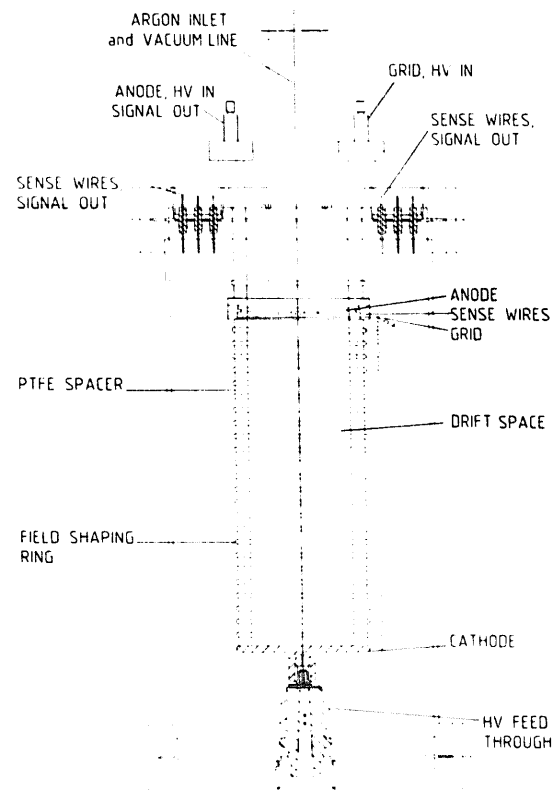

Fig. 4. A cross-section through the chamber.

figuration used, it was not necessary to apply any external voltage to the grids.

The two flanges were sealed with copp O-rings, and the whole assembly was baked out under vacuum for 48 h at 100 °C. A relatively low temperature was used to avoid damage to the ceramic resistors. After this procedure a typical leak test rate was 5×10^{-9} mbar l s^{-1}, and the outgassing rate of the chamber was 1×10^{-13} mbar l s^{-1} cm^{-2}. Published values for the outgassing of stainless steel (obtaned using different cleaning procedures) range from about 5×10^{-12} to 10^{-13} mbar l s^{-1} cm^{-2} [16].

3. The purification system

The purification system has been described in detail in a previous publication [9]. The same procedure for liquefaction was followed as described in ref. [9], with the rate of liquefaction into the chamber being about 1 litre of liquid per hour. Prior to allowing any liquid into the chamber, the latter was slowly cooled until the external temperature of the plot reached about −100 °C. This was a precaution to prevent wires breaking on coming into contact with the cold argon entering the chamber.

4. Experimental setup: electronics and data acquisition

Data were taken with the chamber placed in a 5 GeV pion beam at the CERN proton synchrotron (PS). A schematic of the experimental setup and readout system is shown in fig. 5. The trigger was defined by five scintillation counters placed in coincidence. The vertical spread of the beam entering the chamber was limited by a "finger" counter of dimensions $80 \times 5 \times 5$ mm^3. The accelerator produced one burst of particles of 500 ms duration every 10 s, and the number of triggers per burst in the five counters was ≈ 6. This rate gave typically one track recorded in the chamber per trigger. The chamber was placed in an open dewar of liquid argon for each of refilling, and both were then placed on a platform which enabled the position and height of the chamber with respect to the beam to be adjusted.

A schematic of the front-end electronics together with the connections to the chamber is shown in fig. 6. The signals induced on the sense-wires were brought out of the chamber through 120 cm long commercial coaxial cables. These long cables had the disadvantage of increasing the input capacitance of the amplifier to 120 pF (110 pF due to the coaxial cable and 10 pF real detector capacitance), and also to make the amplifier more sensitive to microphonic noise. This type of noise had two main sources. The first was mechanical vibrations from outside the detector, this contribution was found to be negligible in the operational environment at the CERN PS test beam. The second source of microphonic noise arose from argon gas bubbles around the coaxial cables caused by boiling of the liquid argon in the bath around the chamber. Vertical aluminium tubes long enough to stay above the liquid argon level were mounted on each feedthrough and filled with paraffin wax. In this way the cables were no longer in contact with the liquid argon, and at the same time all the connections were mechanically reinforced.

The sense-wire amplifier was of the charge sensitive type and had a rise time and decay time constant of 1 μs and 40 μs respectively. Laboratory tests made using a 1 μs shaping time, gave the following noise characteristics: ⟨ENC⟩ = 330 electrons for 0 pF input capacitance and a slope of 2.26 electrons/pF.

Tests made in actual working conditions without using any shaping circuit gave the following results: ⟨ENC⟩ = 600 electrons for $C_{in} = 0$ pF, and ⟨ENC⟩ = 1300 electrons for $C_{in} = 120$ pF.

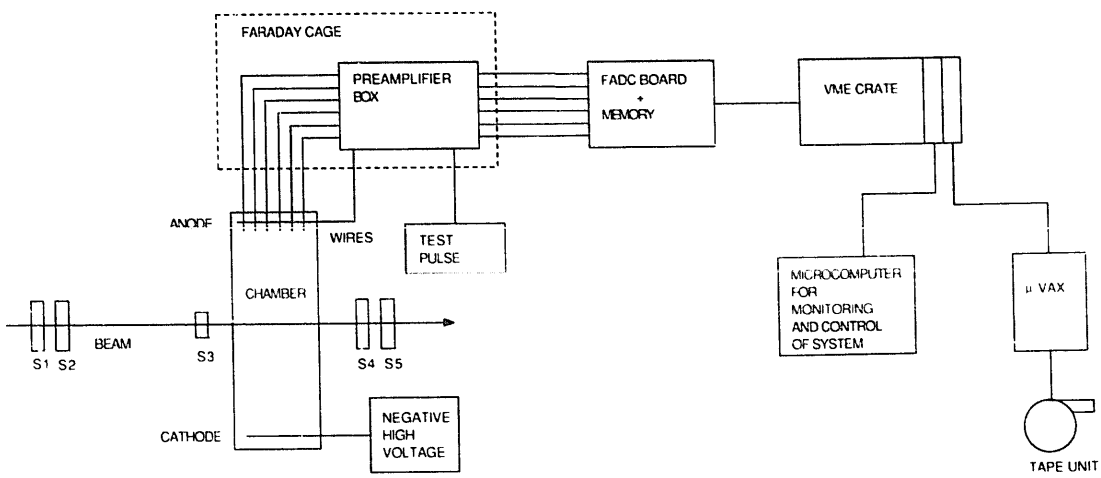

Fig. 5. A schematic of the experimental setup and readout system.

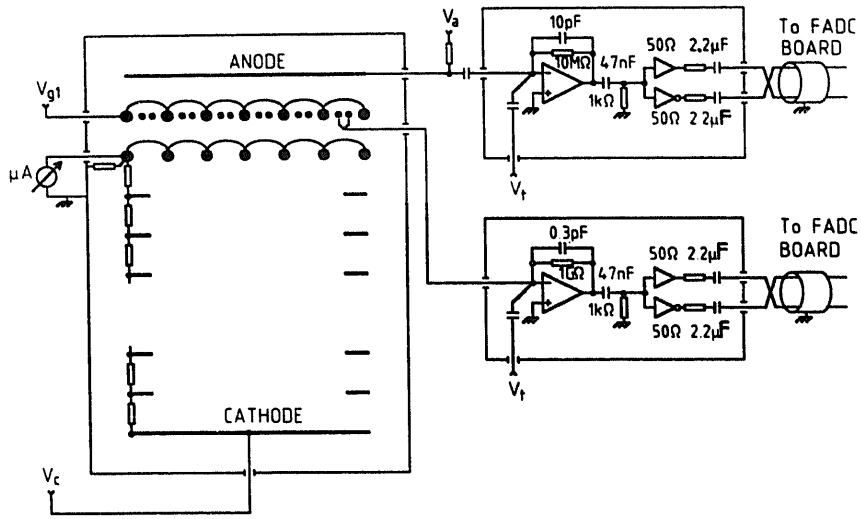

Fig. 6. A schematic of the front-end electronics, showing the connections to the chamber.

This noise figure corresponds to a signal-to-noise ratio of 4.5 for a signal of 6000 electrons. We did not use any shaping circuit, because of the triangular shape of the induced signal. A shaper would have caused the loss of the rise time information of the induced signal. The gain of the amplifier was 56 mV/fC. A test pulse could be injected through a 1 pF test capacitor to determine the calibration factor. We used a test pulse of amplitude 1.6 mV giving an input charge of 10000 electrons.

The anode was also connected to an amplifier and this could be read out to obtain the total charge deposited on the wires. We used the same amplifier as for the sense-wires, but with a longer decay time of 80 μs, and reduced gain to prevent saturation of the signals.

The sense-wires amplifiers were housed in two boxes, each box containing 16 amplifiers. The anode amplifier was in an individual box together with its high voltage (V_a in fig. 6) decoupling capacitor and the biasing resistor. The three boxes were in turn placed in a Faraday cage, and a supplementary shield was put around the signal cables. The cage was located next to the chamber to minimize cable length.

After the preamplifier stage, the signals were passed on to a digitizer board [17]. The board contained 40 channels, each channel consisted of a line receiver, an 8 bit flash ADC and two 8 kbyte × 8 memories. The flash ADC digitized continuously at a rate of 5 MHz and stored the information in the first 8k memory. After a trigger, a delay of 1.6 ms was generated. At the end of the delay a stop signal was supplied and digitizing ceased. The data were then transferred to the second 8k-memory for reading by the VME system. One could either read out the complete 8k of memory after the stop signal, or else only part of the memory. When a trigger arrived, a test pluse was generated and was digitized along with the event to indicate the start of drift.

The data acquisition system was VME based and was controlled using Macintosh microcomputers [18]. The VME crate was also connected to a μVax II via an interface known as VASCO [19]. The data were transferred to the μVax II where they were recorded on magnetic tape for further analysis.

5. Results

A total of about 12000 triggers were recorded at different electric fields and drift distances. At 500 V/cm and 200 V/cm a total of ≈ 1200 triggers were taken at each field and drift distance (nominal values of 40, 80, 120, 160, 220 mm). We also recorded ≈ 14000 triggers at 500 V/cm and 8 cm drift distance to study the production of delta rays.

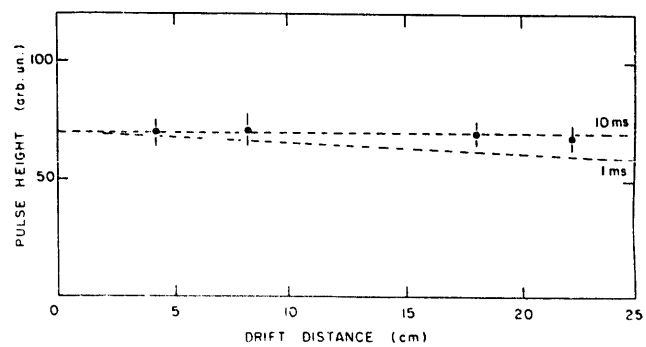

Fig. 7. The pulse height (in arbitrary units) for different distances at 500 V/cm using the chamber as a normal gridded ionization chamber, together with curves for 1 ms and 10 ms.

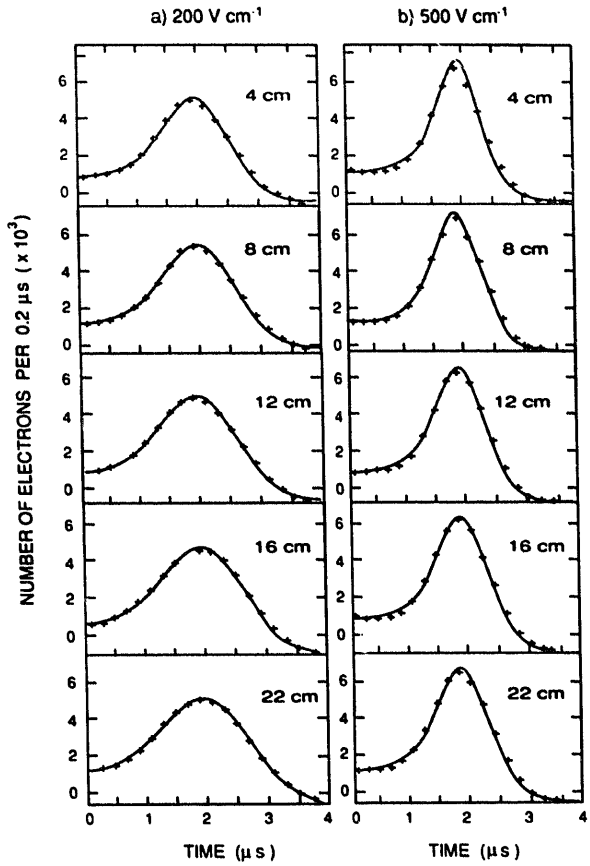

Fig. 8. A series of 10 pulses taken at different drift distances, for (a) 200 V/cm and (b) 500 V/cm. The superimposed curves are the results of the fits described in the text.

5.1. Pulse height and pulse shape measurements

It is clearly important to demonstrate that the observed pulses on the sense-wires are well described by the theoretical shapes given in fig. 3b. Before making any comparisons between the expected pulse shapes and the data, we have checked the quality of the liquid argon by measuring the electron lifetime using data taken at 500 V/cm. The total charge deposited in 2 mm was measured by setting the anode voltage to zero, meaning that the induced signal terminated at the sense-wires. The pulse height as a function of distance is shown in fig. 7 together with curves for τ of 1 and 10 ms, showing that the lifetime is of the order of several milliseconds, as measured in a previous test [9].

We then made fits to the measured pulses using the theoretical pulse shapes. In fig. 8 are shown a series of pulses for the five drift distances and fields of 200 V/cm and 500 V/cm.

The function $F(t_i)$ used to fit the data is a combination of a linear background and the theoretical pulse shape, namely

$$F(t_i) = At_i + B + Hf_{\text{th}}(t_i + T), \quad (3)$$

Table 1
Number of electrons as a function of drift distance and electric field

Drift distance [cm]	Number of electrons	
	200 V/cm	500 V/cm
4	5510±250	6760±190
8	5240±230	6490±270
12	4980±210	6200±240
16	4660±210	6020±200
22	4580±160	5760±170

where t_i is the time corresponding to bin i, A and B are parameters describing the background, H is a scale factor that normalizes the theoretical pulse shape f_{th} to the measured pulse and T is a time offset measured from the trigger time. In order to reduce the effects of the electronic noise on the pulse shape, the pulses at a given field and drift distance have been averaged together. The theoretical shape also included the amplifier response. The resulting fits are shown as the solid curves in fig. 8. The agreement between the measured and fitted pulses is very good.

The measured amplitudes in number of electrons are given in table 1. The pulse height at 200 V/cm is lower than that at 500 V/cm, due to the increased recombination of the electron–ion pairs that takes place at the lower field. In fig. 9 we plot the measured amplitudes as a function of distance.

The amplitudes are lower than expected for two reasons: 1) the induced charge never reaches 100%, the mean value being 75%, 2) due to the rise time of the amplifier the pulse height is reduced by 20%. In addition, the amplitude decreases faster with distance than would be expected by the measured lifetime. This decrease is due to the diffusion of the 2 mm electron

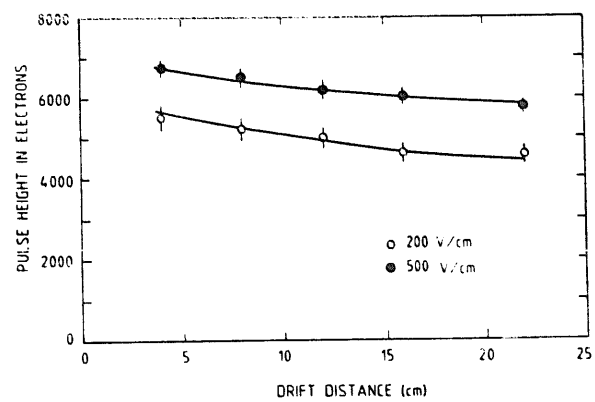

Fig. 9. The pulse height in number of electrons as a function of the drift distance, for 200 V/cm and 500 V/cm. The curves are derived from values of the best fit to each of the pulses in fig. 8.

track. There are two types of diffusion, lateral and longitudinal. The lateral diffusion is not expected to play any role here, as any movement of electrons towards the adjacent sense-wire gap will be compensated by electrons moving in the opposite direction. As the electrons drift across the grid/sense-wire gap there may be some broadening of the electron track, but the effect is expected to be negligible. However, the effects due to longitudinal diffusion will have a more marked effect on the track. The longitudinal spread of the electron track is given by

$$\sigma = \sqrt{2Dt}, \tag{4}$$

where D is the diffusion coefficient and t is time in seconds. For thermal electrons we have the Einstein–Debye relationship, namely

$$D = \frac{k_B T}{e}\mu, \tag{5}$$

where μ is the electron mobility, T is the temperature, k_B is Boltzmann's constant and e is the electronic charge. Making the relevant substitutions in eq. (5) with $T = 87$ K gives $D = 4$ cm^2 s^{-1}. Electrons in liquid argon are thermal, up to electric fields of ≈ 200 V/cm. At higher fields the electrons gain more energy from the field than they lose in collisions with the argon atoms and so become nonthermal, and hence eq. (5) no longer applies. However, for fields ≤ 1 kV cm^{-1} the diffusion coefficient has a constant value of ≈ 4 cm^2 s^{-1}, the low field value. Longitudinal diffusion spreads out the electron track in time, so for a track segment which is parallel to the wire plane the electrons no longer arrive all at the same time. This leads to a broadening of the pulse on the sense-wires, and therefore a reduced pulse height (charge must be conserved). Although this time spread is small (≤ 0.2 μs at 22 cm drift and 500 V/cm), the signal is very narrow, hence even this small spread has a noticeable effect. This spread has been included in the theoretical pulse shapes used to fit the measured pulses. The curves in fig. 9 are obtained from the fitted curves in fig. 8 and include an electron lifetime of 10 ms.

5.2. Measurement of the electron drift velocity

Using the data taken at different drift distances we have measured the drift velocity for electric fields $E = 500$ V/cm and $E = 200$ V/cm. For each electric field and drift distance the position in time of the signal is determined and then averaged over many signals. This average time is plotted as a function of the drift distance in fig. 10 for the two electric fields. We find that due to uncertainties in the measurement of the drift distance there is an offset of 0.8 cm meaning that the 4 cm drift distance is actually 3.2 cm. This offset has been

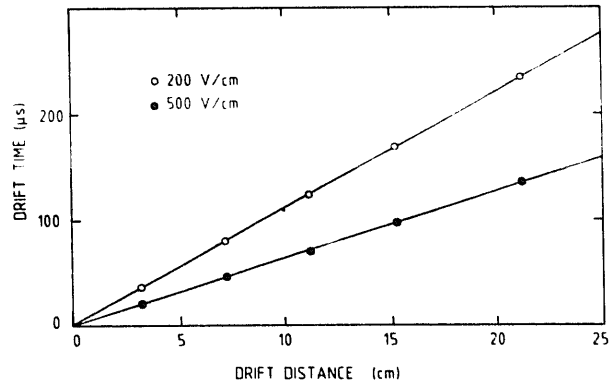

Fig. 10. The drift time for 200 V/cm (○) and 500 V/cm (●) as a function of drift distance. The data have been corrected for the 0.8 cm offset described in the text. The curves are a straight line fit of the form $d = v_d t_d$, and give $v_d = 0.89$ mm μs^{-1} for 200 V/cm and $v_d = 1.55$ mm μs^{-1} for 500 V/cm.

corrected for when plotting the data in fig. 10. The curves are a straight line fit of the form

$$d = v_d t_d, \tag{6}$$

and yield $v_d = 1.55$ mm/μs at 500 V/cm and $v_d = 0.89$ mm/μs at 20 V/cm. These values compare well with values determined previously by us [9] and by other authors [7,20–24].

5.3. Observation and measurement of delta rays

One of the purposes of the ICARUS experiment [8] is to detect and measure the recoil electrons from the interaction of solar neutrinos within the detector volume. It is therefore important to be able to identify and measure electrons with energies of a few MeV.

A particle travelling through matter leaves a trail of electron–ion pairs along its path. If the liberated electrons have sufficient energy then they may form an independent track, creating a further series of electron–ion pairs. These electron tracks are referred to as delta rays. The kinetic energies of the recoil electrons from the interactions of neutrinos from the ^{8}B cycle in the sun are in the range 0–13.5 MeV, similar to the energies of the delta rays that will be contained in the chamber.

An incident particle of kinetic energy T can lose energy up to a value T_{max}, where

$$T_{max} = \frac{2m_e\gamma^2\beta^2}{\left(1 + 2\gamma(m_e/m) + (m_e/m)^2\right)}, \tag{7}$$

with m_e = electron rest mass, $\beta = v/c$ = velocity of incident particle, m = mass of incident particle. For a pion of momentum 5 GeV/c this maximum energy loss is 1 GeV. The number of electrons of energy $T \ll T_{max}$ produced per cm per unit energy is [25]:

$$\frac{d^2N}{dT\,dx} = \tfrac{1}{2}D\left(\frac{Z_{med}}{A_{med}}\right)\left(\frac{Z_{inc}}{\beta}\right)\rho_{med}\frac{1}{T^2}, \tag{8}$$

where $D = 0.307$ MeV cm^2 g^{-1}, Z_{med} and A_{med} are the atomic number and mass respectively (which for argon are 18 and 40), ρ_{med} is the density of the medium (1.4 g/cm^3 for liquid argon) and Z_{inc} is the charge of the incident particle. For $T \approx T_{max}$ there are corrections to eq. (8) arising from the spin of the incident particle. Integrating eq. (8) over x (= 6.2 cm) gives

$$\frac{dN}{dT} = \frac{0.6}{T^2}. \tag{9}$$

Hence the number of delta rays with energies greater than T_{min} produced per pion is

$$N(T_{min} < T < T_{max}) = 0.6\left(\frac{1}{T_{min}} - \frac{1}{T_{max}}\right). \tag{10}$$

For $T \ll T_{max}$ the number of delta rays per pion is given by $0.6/T_{min}$, hence for $T_{min} > 1$ MeV, 60% of the events should contain a delta ray.

The data sample used for this measurement was 14276 events taken at 500 V/cm and 8 cm drift distance. An event was considered to contain a delta ray candidate if there was a second track, connected to the main track of the pion, with at least two pulses separated from the main track by at least 4 mm. For 500 V/cm the drift velocity was 1.55 mm μs^{-1}, so 4 mm separation corresponded to 13 time bins where one time bin was 200 ns. Four typical events selected in this way are shown in fig. 11. The pion track occurs between 70 and 80 μs, as expected for the 8 cm drift distance. The track at 27 μs is a test pulse (generated with the trigger) which indicates the start of drift. The delta rays appear as distinct tracks at an angle to the pion track. The direction of the pion is from wire 31 to wire 1. To obtain the energy of the delta ray we sum up the energies of the individual pulses satisfying the above criteria. The presence of only one space coordinate makes it difficult to extract any reliable measure of the angle of emission of the electron, although the energy can still be determined.

It is often difficult to identify the start of the delta ray, as it may be superimposed on the pion track. Also, multiple Coulomb scattering can considerably distort the path of the electron. Hence the requirement on the pulse separation means that we do not reconstruct all the energy deposited by the delta ray. To study this energy loss we have used a Monte Carlo to generate events containing delta rays of a given energy and have simulated the effects of the multiple scattering. The events are then passed through our drift chamber simulation program. Two such events are shown in fig. 12, generated with energies of 10 MeV (fig. 12a) and 15 MeV (fig. 12b) respectively. We then apply the same

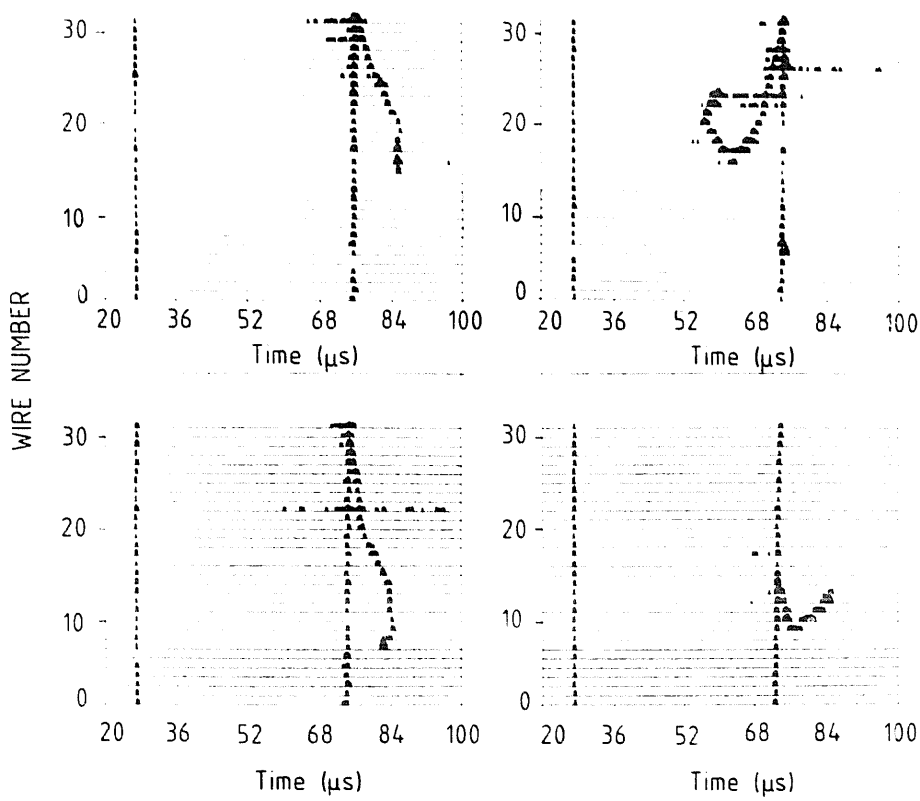

Fig. 11. Four typical events containing delta ray candidates. The track at 27 μs is a test pulse and indicates the start of the drift time. The track between 70 μs and 80 μs is that of the pion, and the delta ray can be clearly seen emerging at an angle from the main track.

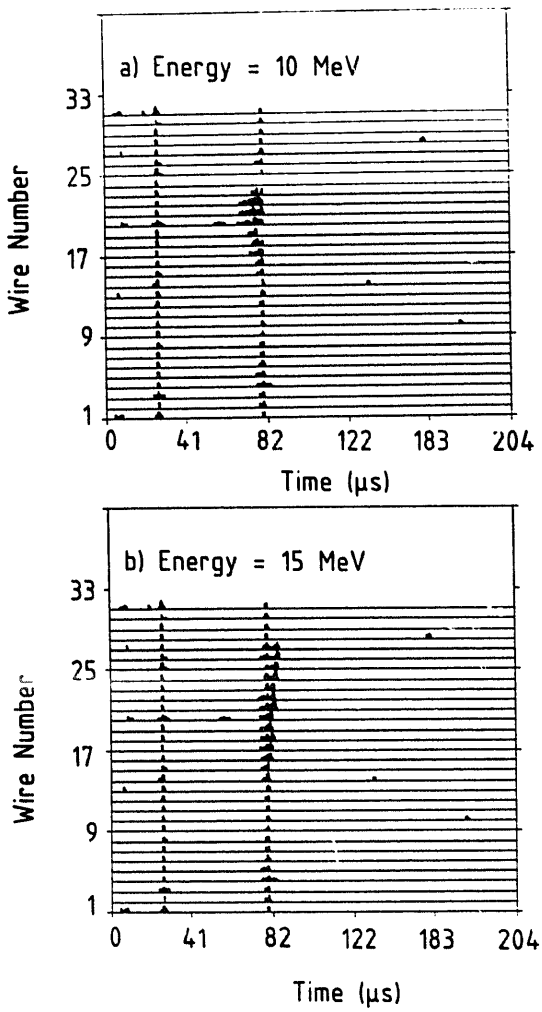

Fig. 12. Two examples of Monte Carlo events containing delta rays after simulation of the drift chamber. The track at ≈ 27 μs is a test pulse and indicates the start of the drift time. The track at 82 μs is the pion track. The generated energies of the delta rays are (a) 10 MeV and (b) 15 MeV.

selection criteria to our Monte Carlo events, compute the visible energy for each event, and compare it to the generated energy. This is repeated for many events and the mean visible energy is calculated. Fig. 13 shows the curve obtained for generated energies from 1.5 to 23 MeV. The percentage of energy seen is not a constant but varies from 40% for a generated energy of 5 MeV to 63% for a generated energy of 23 MeV. We then use this curve to correct the data.

Using the Monte Carlo we can also determine the acceptance of the events as a function of electron energy. Several factors contribute to reduce the acceptance to less than 100%. Firstly, low energy electrons are difficult to identify as they may only contribute one pulse with more than 4 mm separation from the pion track. Secondly, the single wire plane means that for certain angles of emission of the electron it will not be

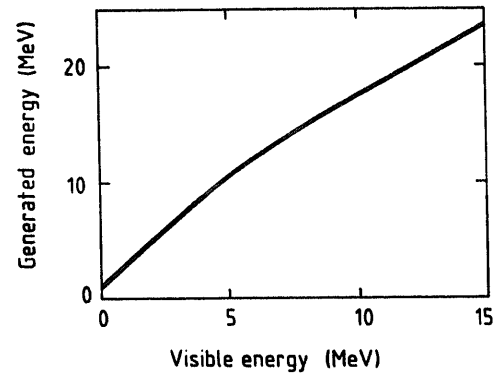

Fig. 13. The visible energy of the delta rays for a given generated electron energy. Only those electrons producing at least two pulses separated from the main track by at least 4 mm are included in the calculation of the visible energy.

seen as a separate track. Problem configurations are, 1) electrons in the same vertical plane as the pion, and 2) electrons emitted parallel to the sense-wires. In the first case the electron track will be superimposed on that of the pion, and in the second case it will deposit all of its charge on one wire. Thirdly, due to the limited fiducial volume, high-energy electrons will not be contained in the chamber. For this reason we restrict our sample to those events where there are no pulses on wires 1 or 31 that contribute to the delta ray. In fig. 14 we show the acceptance curve for the selection criteria. For an electron energy of 5 MeV the acceptance is 37%, falling to 16% at 20 MeV due to electrons not contained in the chamber. For energies below 3 MeV the acceptance is less than 1%, and between 1.5 MeV and 3 MeV it falls by two orders of magnitude, making the acceptance in this region rather uncertain.

The fully corrected data are shown in fig. 15 together with the theoretical prediction (error bars are statistical

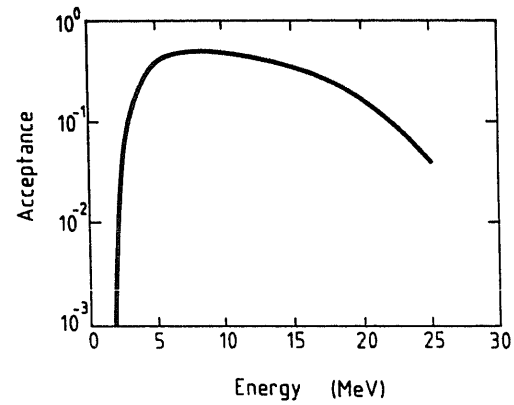

Fig. 14. The acceptance curve as a function of the delta ray energy for the 4 mm separation and at least two pulses produced. The decrease at low energy is due to the requirements on pulse separation and number of pulses. The subsequent decrease at higher energies is due to electrons that are not fully contained in our sensitive volume.

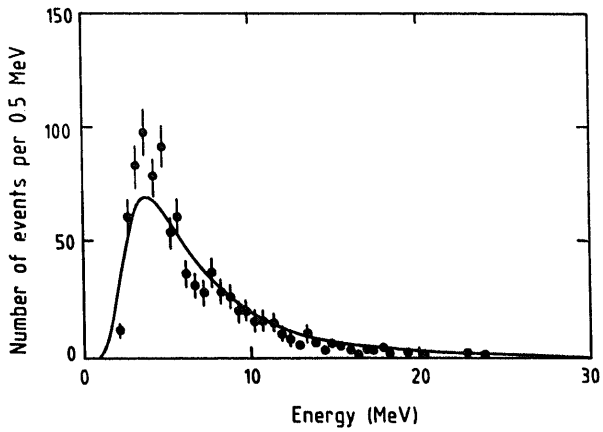

Fig. 15. The fully corrected energy spectrum for the delta rays (error bars are statistical only). The curve is the theoretical prediction from eq. (9) and includes the total number of events N_{tot} and the acceptance from fig. 14.

only). The curve has been obtained from eq. (9), and includes the acceptance from fig. 14 and the total number of events N_{tot}. Above 5 MeV the curve gives a good description of the data. In the peak the Monte Carlo predicts less events than are actually observed, but as has been noticed the acceptance in this region is falling very fast and is probably less reliable. In addition there is a systematic error on the energy scale of +10% due to uncertainties in the absolute calibration.

Our final data sample contains 880 events. The expected number of events N can be obtained from eq. (9):

$$N = N_{tot}\, 0.6 \int_{T_{max}}^{T_{min}} A(T) \frac{1}{T^2} dT, \qquad (11)$$

where $A(T)$ is the acceptance as a function of energy. The limited acceptance reduces the expected percentage of events containing delta rays from 60 to about 6%. This gives the expected number of events as 892, which is in good agreement with the observed number of events.

6. Conclusions

We have tested a liquid argon TPC containing a sense-wire plane to obtain nondestructive detection of the electron image of ionizing events. The novel wire configuration was based on the principle of electrostatic focussing. The measured pulse shapes at both 200 and 500 V/cm were in very good agreement with the expected shapes, calculated taking into account the electron lifetime, the response of the electronics and the longitudinal diffusion of the 2 mm electron cloud. The measured electron drift velocity was in good agreement with the results of other workers as well as with our previous measurements.

In addition, we have selected a sample of delta rays in order to study the behaviour of low-energy electrons in the liquid argon. We find that for electron energies greater than 5 MeV the measured and predicted spectrums agree very well after the acceptance and energy losses have been corrected for, demonstrating the feasibility of recognizing low-energy electrons.

We have demonstrated that the idea of electron imaging using grids of wires works as expected. We obtained clear signals above the electronic noise (signal-to-noise ratio of 4.5) for a signal of 6000 electrons. This is clearly an important step in the realization of the ICARUS experiment, and we now plan to construct a full-scale prototype based on this wire design.

Acknowledgements

We gratefully acknowledge the support of the Istituto Nazionale di Fisica Nucleare in funding this work. Thanks are also due to the following people who have helped in the preparation of the work described here: L. Bassi, M. Benveruto, A. Bochaton, M. Cicia, C. Detraz, A. Galvagni, K. Morgan, J. Oliver, R. Pavanello and R. Truhan.

References

[1] C. Rubbia, CERN-EP Internal Report 77-8 (1977), unpublished.
[2] H.H. Chen and J.F. Lathrop, Nucl. Instr. and Meth. 150 (1978) 585.
[3] H.H. Chen and P.J. Doe, IEEE Trans. Nucl. Sci. NS-28 (1981) 454.
[4] P.J. Doe, H.J. Mahler and H.H. Chen, Nucl. Instr. and Meth. 199 (1982) 639.
[5] K. Dieters et al., Nucl. Instr. and Meth. 180 (1981) 45.
[6] E. Gatti et al., IEEE Trans. Nucl. Sci. NS-26 (2) (1979) 2910.
[7] E. Aprile, K.L. Giboni and C. Rubbia, Nucl. Instr. and Meth. A241 (1985) 62.
[8] ICARUS proposal, INFN/AE-85/7 Frascati (1985); Proposal for the ICARUS experiment phase 1, CERN-Frascati-L'Aquila-Padova-UCLA Collaboration (1988), LNF-89/005(R).
[9] E. Buckley et al., Nucl. Instr. and Meth. A275 (1989) 364.
[10] Messer Griesheim GmbH, Oxisorb Gas purifying system.
[11] A. Gonidec et al., CERN-EP/88-36 (1988), submitted to Nucl. Instr. and Meth.
M. Albrow et al., Nucl. Instr. and Meth. A265 (1988) 303.
[12] O. Bunemann, T.E. Cranshaw and J.H. Harvey, Can. J. Res. 27 (1949) 191.
[13] This procedure was originally developed for the cleaning of the stainless steel vacuum elements of the CERN intersecting storage rings. See A.G. Mathewson, CERN-ISR-VA 74-10 and 74-30, unpublished;

M-H. Achard, R. Calder and A.G. Mathewson, Vacuum 29 (2) (1978) 53.
[14] MACOR is a machinable glass ceramic made by Corning.
[15] ConFlat is a trademark of Varian, USA.
[16] Y. Strausser, Review of Outgassing Resutls, technical report VR-51 (Vacuum Division, Varian Associates, 1968).
[17] The digitizer board was designed and constructed by J. Oliver, Harvard University, USA.
[18] Macintosh is a trademark of Apple Computer Inc, USA.
[19] VASCO is an interface between μVax and VME developed jointly at the Universities of Padova and Pavia, Italy.
[20] K. Yoshino, U. Sowada and W.F. Schmidt, Phys. Rev. A14 (1976) 438.
[21] E. Shiburama et al., Nucl. Instr. and Meth. 131 (1975) 131.
[22] L.S. Miller, S. Howe and W.E. Spear, Phys. Rev. 166 (1968) 871.
[23] B. Halpern, J. Lekner, S. Rice and R. Gomer, Phys. Rev. 156 (1967) 351.
[24] E.M. Guschchim, A.A. Kruglov and I.M. Obodovskii, Zh. Eksp. Teor. Fiz. 82 (1982) 1114.
[25] Review of particle properties, Phys. Lett. 170B (1986).